Landmark-Based Virtual Path Estimation for Assisted UAV FPV Tele-Operation with Augmented Reality

Santiago Grijalva[1] and Wilbert G. Aguilar[1,2,3](✉)

[1] CICTE, Universidad de las Fuerzas Armadas ESPE, Sangolquí, Ecuador
wgaguilar@espe.edu.ec
[2] FIS, Escuela Politécnica Nacional, Quito, Ecuador
[3] GREC, Universitat Politècnica de Catalunya, Barcelona, Spain

Abstract. In this paper we proposed an Assisted UAV Tele-Operation System, specifically for FPV navigation based on Artificial Landmarks in obstacle free environments. The system estimates the optimal path through landmarks and traces an artificial route to be followed. Path recognition uses color space and morphological transformation such as eroding and dilating to reduce noise due to different lighting environments. Once path is recognized ORB detector is used for getting a set of the most representative pixels coordinates, this is done for each ROI (Region of Interest) in the camera image. Later, the median of each pixel coordinate in the specific ROI is considered for interpolation needed to trace the route. Parrot's drone Bebop 2 was used for the purpose of this study as it has a fisheye lens camera that allows us to face downwards to detect the landmarks.

Keywords: UAV · Tele-Operation · Augmented reality · Landmark

1 Introduction

Unmanned Aerial Vehicles (UAVs) [1, 2] are widely used in recent applications such as 3D mapping [3, 4], topographic survey [5], precision farming [6], surveillance systems [7–10], rescue, military reconnaissance [11, 12], disaster area identification, etc. [13–16]. Most of this applications show advance in fully autonomous UAVs [17–19], but human-machine interfacing will always be present for specific applications, therefore development of efficient assistance systems during flights it is critical and shall be capable to give enough information to the tele-operator for a prompt response.

Vehicle teleoperation first appeared in the early 1900s but it was not until the 1970s that systems became widely used [20]. Since then tele-operation has been dependent on operator's expertise and requires training, especially when First Person View (FPV) mode limits the operator's field of view, decreasing awareness of the environment.

Nowadays augmented and virtual reality applications are used mostly for general entertainment. DronePrix AR by EdgyBees is an Augmented Reality application for DJI's Drone Mavic Pro that allows the user to interact with a virtual racing track. Furthermore, there are other types of application [21–23] such as Augmented Reality

H. Yu et al. (Eds.): ICIRA 2019, LNAI 11745, pp. 688–700, 2019.
https://doi.org/10.1007/978-3-030-27529-7_58

Maps or Augmented Reality (AR) for drone navigation. The present document resides in the last study case; we propose a system that allows the tele operator to be aware of that path that must be followed making use of an estimated landmark-based virtual path [13, 24, 25] traced in arrow shape in an AR application.

This paper is organized as follows: Sect. 2 presents a quick review of the literature about Vehicles Teleoperation and the different approaches to offer full guidance, security and comfort to the tele-operator. Section 3 presents our first approach to give the tele operator assistance during a UAV flight, despite of being addressed to artificial landmarks at first, it can be easily used on natural landmarks or paths; experimental results and test conditions, in addition, a comparison with hand-traced optimal path are presented in Sect. 4. conclusions and future work are presented in the last section.

2 Related Works

Bilateral systems for UAV teleoperation [26] are very common [27–29] as they may involve time delay due to signal loss, Lam et al. presented a study for obstacle avoidance in a tele operation system for a UAV that had a response delay to tele operator commands.

Military applications for UAVs are the most common due to their ability to navigate in complex environments. Chen in 2010 [30] presented a simulation of a military reconnaissance environment where the UAV showed exocentric vision of the whole space while the Unmanned Ground Station (UGV) showed egocentric perspective of the environment [31]. This study case is very different from others as the tele operation resides on the UGV while the UAV assists giving an overview visual feedback.

Haptic and visual feedback started to lead in assisted teleoperation systems, in [27, 32–34] presented bilateral haptic teleoperation of under actuated UAV, in [32] tele operator receives haptic feedback from the environment as a function of the distance to an obstacle or the approach rate.

Lee et al. [28, 35] presented a novel haptic teleoperation control framework for multiple UAVs, this framework consists of three layers, UAV control layer, Virtual Point Control Layer and the teleoperation layer in which the tele operator is capable to drive one or all the UAVs present in the framework.

Studies for natural path recognition are important to provide the tele-operator trust information. Approaches based on monocular camera such as [36, 37] achieved very accurate results. [38] Detected paths based on monocular images from a ground robot named ExaBot, this study includes horizon detection based on morphological transformation and path detection based on color transformations. Even though this is not guided for assisted teleoperation is similar to our study.

Obstacle detection [39] and object tracking [21, 40] is as well important for guidance in UAV as it provides valuable information about the environment, feature point detection approaches had been used to detect obstacles or track objects and landmarks [38, 39, 41].

Aleotti et al. implemented an Augmented Reality Interface that allows a tele-operator to be aware of the environment while the UAV equipped with a gamma-ray detector alert of possible nuclear radiation sources in the display [42].

3 Our Approach

Our system consists of three main factors: Tele-operator, Parrot Bebop 2.0 and a ground station (GS). Image processing is done off-board in the GS. UAV connects to the GS through a Wi-Fi signal emitted by itself. Then a *nodelet* is raised in the ground station letting the drone publish ROS Messages, specifically it publishes the video capture in *image_raw* topic as a *sensor_msgs/Image* message. To convert ROS Images we use *cv_bridge* that let us interface directly with the video capture on OpenCV. After image processing, estimated virtual path is presented to the tele-operator in GS's screen to send control commands depending on the UAV positioning in relation to the artificial route (Fig. 1).

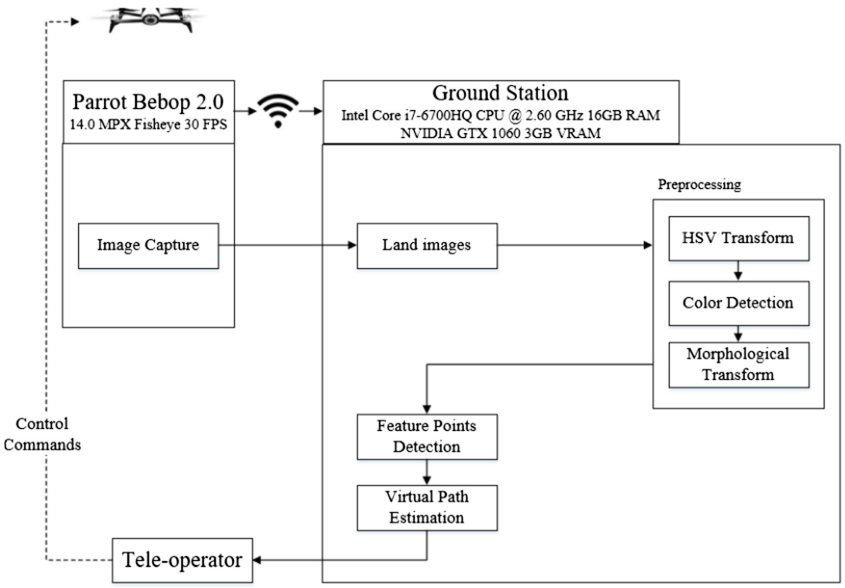

Fig. 1. Proposed system overview

The proposed system makes use of an input image (856 × 480 pixels) from a monocular camera facing downwards to obtain a processed image with the artificial path to be followed by the tele-operator. For this, the following steps must take place in image processing:

3.1 Color Space Transformation and Color Detection

The input image obtained from the UAV's camera needs to be transformed from the BGR color space to HSV color space. This is widely used in applications that detect a specific color with different brightness and saturation levels, thus HSV help us

achieving acceptable results in different lighting conditions. Figures 2, 3 and 4 show raw image and masked input image for three different lighting levels.

Fig. 2. Raw image from UAV's camera (Left) and masked input image (Right) for $\sim$ 10000 lx (Color figure online)

Fig. 3. Raw image from UAV's camera (Left) and masked input image (Right) for $\sim$ 2000 lx (Color figure online)

Fig. 4. Raw image from UAV's camera (Left) and masked input image (Right) for $\sim$ 300 lx (Color figure online)

3.2 Morphological Transformation

Once color was successfully detected, erode transformation takes place first to reduce noise that might have been miss-detected in the previous step, as it erodes the boundary of the foreground object by the size of the kernel, in this study a 2×2 kernel was used.

Next, a dilation transform is applied to the eroded one, to increase the size of the landmarks that have been almost eroded. This method is also known as Opening Transformation. Algorithm 1 summarizes the proposed preprocessing method.

Algorithm 1: Input image preprocessing

1: Read *image* from Bebop 2
2: **if** *image* **not** *Nule* **then**
3: *hsv_image* = **brg8_to_hsv**(*image*)
4: *mask* = **inRange**(*hsv_image, upper_limit, lower_limit*)
5: *erosion* = **erode**(*mask, kernel*)
6: *dilation* = **dilate**(*erosion, kernel*)

Parameters	
image:	Raw input image
upper_limit:	HSV upper color limit for color detection
lower_limit:	HSV lower color limit for color detection
kernel:	2x2 ones matrix for erode and dilate functions
Functions	
bgr8_to_hsv:	Converts input image from BGT color space to HSV color space
inRange:	Filters all pixels which pixel's intensities are not in the range established by *upper_limit* and *lower_limit*
erode:	Erodes the input image
dilate:	Dilates the input image

3.3 Feature Points Detection

To reduce the number of pixels obtained in the previous step, ORB OpenCV's algorithm was used to detect feature points. We divided the image obtained in the previous step in different regions of interest. Then detection takes place for each ROI (Fig. 5), drastically reducing the number of points to be processed. Once a max number of 100 points is detected for each ROI, median point of the set for each ROI is considered for the route interpolation, as it is not biased by noise that might have not been filtered in the previous steps.

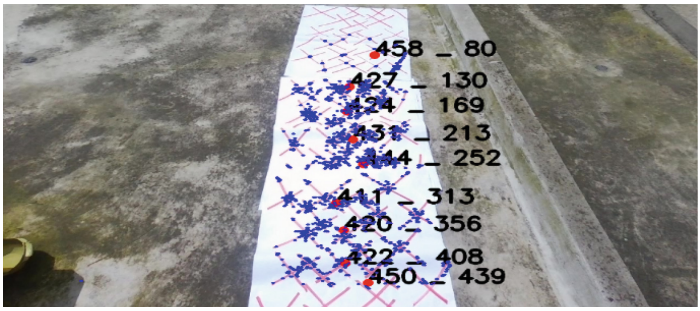

Fig. 5. ORB feature points (Blue) and median point for each ROI (Red) (Color figure online)

Algorithm 2: Feature point detection and median calculation for each ROI

```
Divide image in n ROIs
for each ROI :
  feature_points = orb_detect(image)
    if length(feature_points) > threshold then
      x_median = median(feature_points_x)
      y_median = median(feature_points_y)
      std_x = std(feature_points_x)
      std_y = std(feature_points_y)
      append x_median to new_x_points
        append y_median to new_y_points
    end if
end for
```

Parameters	
image:	Preprocessed image
n:	Number of ROIs
threshold:	Minimum number of features to calculate median and standard deviation for ROI

Functions	
ord_detect:	Detects feature points using ORB detector
length:	Calculates size of vector
median:	Calculates median for the input vector
std:	Calculates standard deviation for the input vector
append:	Appends a value to a vector

3.4 Route Tracing

From points detected for each ROI in the previous step, a polynomial regression is done in real-time. To avoid excessive refreshing of the traced route that might end up in misunderstanding to the tele-operator, the following algorithm is applied:

Algorithm 3: Route tracing and refreshing

```
Store previous points as old_points
Calculate new_points using Algorithm 2
if length(new_x_points ) > length(old_x_points) then
   old_points = new_points
else if length(new_x_points) < length(old_x_points) then
   old_points = new_points
else
   for each point in new_points
      if new_point_x > old_point_x + 2*std_x then
         old_point_x = new_point_x
      else new_point_x < old_point_x – 2*std_y then
         old_point_x = new_point_x
      end if
   end for
end if
Repeat 3 to 16 for new_y_points
Polynomial regression with old_x_points and old_y_points
Evaluate x_points with obtained polynomial
Trace estimated virtual path
```

Parameters	
std_x:	Standard deviation for x pixel coordinate
std_y:	Standard deviation for y pixel coordinate
Functions	
length:	Calculates size of vector

4 Results and Discussion

The proposed system was tested experimentally in several scenarios, we defined them as follows (Figs. 6, 7 and 8):

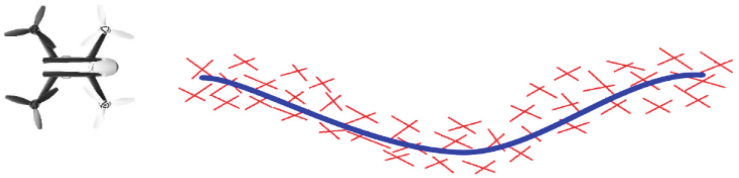

Fig. 6. Smooth curve like artificial landmark path (Color figure online)

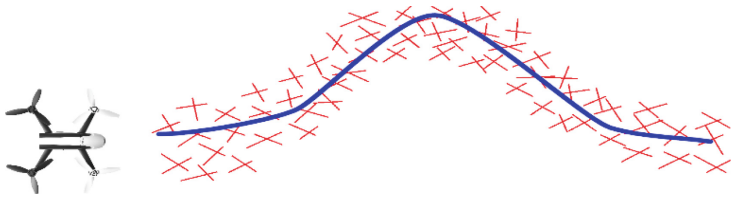

Fig. 7. Sharp bend like artificial landmark path (Color figure online)

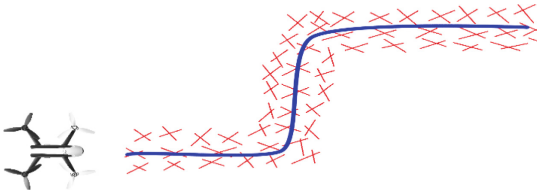

Fig. 8. Left and right turn like artificial landmark path (Color figure online)

a. Route design: It refers to the path formed by the artificial landmarks. Three possible routes were considered: (a) Smooth curve, (b) Sharp bend, (c) Left and right turn.
b. Height: The distance between the UAV and the ground: (a) 1.7 m, (b) 2 m, (c) 2.3 m.
c. Lighting level: The average illuminance depending of the environment: (a) Outdoor Full Daylight $\sim$10000 lx, (b) Outdoor Midday Light $\sim$2000 lx, (c) Outdoor Night Light $\sim$300 lx.

Merging all different conditions, we get 27 possible scenarios. For each one a video capture is recorded for later offline processing. We sample each video capture in 10 different most representative frames, an optimal route is hand traced in OpenCV then the algorithm runs for the same frames and takes the Root Mean Squared Error (RMSE) described by Eq. (1).

$$RMSE = \sqrt{\frac{1}{n}\sum_{i=1}^{n}\left(\widehat{Y}_i - Y_i\right)^2} \tag{1}$$

where

RMSE: Root mean squared error
n: Number of frames
$\widehat{Y}_i$: Estimated path i-th point
Y_i: Optimal path i-th point

Tables 1, 2 and 3, present the mean of RMSE in pixels for each video capture.

Table 1. Mean RMSE for 10 frames of each video capture for Route 1

Lighting level	Height 1: 1.7 m	Height 2: 2 m	Height: 2.3 m
~10000 lx	7.44	8.08	6.49
~ 2000 lx	7.62	6.59	5.36
~ 300 lx	8.59	5.65	4.71

Table 2. Mean RMSE for 10 frames of each video capture for Route 2

Lighting level	Height 1: 1.7 m	Height 2: 2 m	Height: 2.3 m
~10000 lx	7.55	5.06	5.14
~ 2000 lx	9.64	7.29	5.61
~ 300 lx	8.29	8.05	6.13

Table 3. Mean RMSE for 10 frames of each video capture for Route 3

Lighting level	Height 1: 1.7 m	Height 2: 2 m	Height: 2.3 m
~10000 lx	9.61	8.3	7.39
~ 2000 lx	13.72	12.86	8.76
~ 300 lx	12.85	6.94	6.15

Tables 4, 5 and 6 present absolute error for total length of the estimated virtual path, relative to the length of the diagonal obtained from the image resolution (856 × 480) calculated as follows:

$$d = \sqrt{h^2 + w^2} \tag{2}$$

where

d: Diagonal length in pixels
h: Height of raw image in pixels
w: Width of raw image in pixels

Table 4. Absolute relative error for path length in Route 1

Lighting level	Height 1: 1.7 m	Height 2: 2 m	Height: 2.3 m
~10000 lx	1.72	1.79	1.29
~ 2000 lx	2.32	2.13	0.83
~ 300 lx	2.67	2.25	0.91

Table 5. Absolute relative error for path length in Route 2

Lighting level	Height 1: 1.7 m	Height 2: 2 m	Height: 2.3 m
~10000 lx	2.50	1.32	1.24
~ 2000 lx	4.17	2.78	1.65
~ 300 lx	2.82	2.81	1.41

Table 6. Absolute relative error for path length in Route 3

Lighting level	Height 1: 1.7 m	Height 2: 2 m	Height: 2.3 m
~10000 lx	1.70	1.71	2.05
~ 2000 lx	4.88	3.2	2.09
~ 300 lx	3.86	2.12	1.24

Figure 9 show a comparison between estimated virtual path and optimal path, blue arrows represent the estimations and red ones represent the hand-traced path, this is the presentation to graphical display to the tele-operator.

Fig. 9. Arrowed line showing the estimated virtual (blue) and optimal (red) path for Sharp Bend (Left) and Smooth Curve (Right) (Color figure online)

5 Conclusions and Future Work

Optimal path estimation through computer vision algorithm makes possible to trace the route according to landmarks positioning, providing assistance for the tele operator to control accurately an UAV during flights. According to Tables 1, 2 and 3 optimal path estimation reduces RMSE as it increases the maximum height, they also show that RMSE increases in lighting levels lower than 2000 lx, tele operator must choose a height over 2 m and environments where there are higher lighting levels than 2000 lx to get more accurate results. Tables 4, 5 and 6 present a minimum percentage error of 0.83% and a maximum of 4.88%, this means that the tele-operator is not going to be aware of the error due to human visual limitations, resulting in trust information to take prompt responses. Estimated virtual path is presented to the tele-operator through a computer display in augmented reality-like application, although there is no more information than the estimated route, this represents a first approach to a complex system where the tele operator gets full environment information. In future works we propose a system that can provide a visual feedback about possible obstacles and estimated route in natural landmarks, specifically in military application, as in this study is not possible to face downwards and forward due to hardware limitations.

References

1. Orbea, D., Moposita, J., Aguilar, W.G., Paredes, M., Reyes, R.P., Montoya, L.: Vertical take off and landing with fixed rotor. In: Chilean Conference on Electrical, Electronics Engineering, Information and Communication Technologies (CHILECON), Pucón, Chile (2017)
2. Orbea, D., Moposita, J., Aguilar, W.G., Paredes, M., León, G., Jara-Olmedo, A.: Math model of UAV multi rotor prototype with fixed wing aerodynamic structure for a flight simulator. In: De Paolis, L.T., Bourdot, P., Mongelli, A. (eds.) AVR 2017. LNCS, vol. 10324, pp. 199–211. Springer, Cham (2017). https://doi.org/10.1007/978-3-319-60922-5_15
3. Aguilar, W.G., Rodríguez, G.A., Álvarez, L., Sandoval, S., Quisaguano, F., Limaico, A.: Visual SLAM with a RGB-D camera on a quadrotor UAV using on-board processing. In: Rojas, I., Joya, G., Catala, A. (eds.) IWANN 2017. LNCS, vol. 10306, pp. 596–606. Springer, Cham (2017). https://doi.org/10.1007/978-3-319-59147-6_51
4. Aguilar, W.G., Rodríguez, G.A., Álvarez, L., Sandoval, S., Quisaguano, F., Limaico, A.: Real-time 3D modeling with a RGB-D camera and on-board processing. In: De Paolis, L.T., Bourdot, P., Mongelli, A. (eds.) AVR 2017. LNCS, vol. 10325, pp. 410–419. Springer, Cham (2017). https://doi.org/10.1007/978-3-319-60928-7_35
5. Basantes, J.: Capture and processing of geospatial data with laser scanner system for 3D modeling and virtual reality of Amazonian Caves. In: IEEE Ecuador Technical Chapters Meeting (ETCM), Samborondón, Ecuador (2018)
6. Pardo, J.A., Aguilar, W.G., Toulkeridis, T.: Wireless communication system for the transmission of thermal images from a UAV. In: Chilean Conference on Electrical, Electronics Engineering, Information and Communication Technologies (CHILECON), Pucón, Chile (2017)
7. Aguilar, W.G., Angulo, C.: Real-time model-based video stabilization for microaerial vehicles. Neural Proc. Lett. **43**(2), 459–477 (2016)
8. Aguilar, W.G., Angulo, C.: Real-time video stabilization without phantom movements for micro aerial vehicles. EURASIP J. Image Video Process. **1**, 1–13 (2014)
9. Aguilar, W.G., et al.: Real-time detection and simulation of abnormal crowd behavior. In: De Paolis, L.T., Bourdot, P., Mongelli, A. (eds.) AVR 2017. LNCS, vol. 10325, pp. 420–428. Springer, Cham (2017). https://doi.org/10.1007/978-3-319-60928-7_36
10. Aguilar, W.G., et al.: Statistical abnormal crowd behavior detection and simulation for real-time applications. In: Huang, Y., Wu, H., Liu, H., Yin, Z. (eds.) ICIRA 2017. LNCS (LNAI), vol. 10463, pp. 671–682. Springer, Cham (2017). https://doi.org/10.1007/978-3-319-65292-4_58
11. Jara-Olmedo, A., Medina-Pazmiño, W., Tozer, T., Aguilar, W.G., Pardo, J.A.: E-services from emergency communication network: aerial platform evaluation. In: International Conference on eDemocracy & eGovernment (ICEDEG) (2018)
12. Jara-Olmedo, A., Medina-Pazmiño, W., Mesías, R., Araujo-Villaroel, B., Aguilar, W.G., Pardo, J.A.: Interface of optimal electro-optical/infrared for unmanned aerial vehicles. In: Rocha, Á., Guarda, T. (eds.) MICRADS 2018. SIST, vol. 94, pp. 372–380. Springer, Cham (2018). https://doi.org/10.1007/978-3-319-78605-6_32
13. Aguilar, W., Morales, S.: 3D environment mapping using the kinect V2 and path planning based on RRT algorithms. Electronics **5**, 70 (2016)
14. Zhang, J., Liu, W., Wu, Y.: Novel technique for vision-based UAV navigation. IEEE Trans. Aerosp. Electron. Syst. **47**(4), 2731–2741 (2011)
15. Zhang, C., Kovacs, J.M.: The application of small unmanned aerial systems for precision agriculture: a review. Precis. Agriculture **13**(6), 693–712 (2012)

16. Nex, F., Fabio, R.: UAV for 3D mapping applications: a review. Appl. Geomat. **6**(1), 1–15 (2013)
17. Aguilar, W.G., Angulo, C., Costa-Castello, R.: Autonomous navigation control for quadrotors in trajectories tracking. In: Huang, Y., Wu, H., Liu, H., Yin, Z. (eds.) ICIRA 2017. LNCS (LNAI), vol. 10464, pp. 287–297. Springer, Cham (2017). https://doi.org/10.1007/978-3-319-65298-6_27
18. Aguilar, W.G., Salcedo, V.S., Sandoval, D.S., Cobeña, B.: Developing of a video-based model for UAV autonomous navigation. In: Barone, D.A.C., Teles, E.O., Brackmann, C. P. (eds.) LAWCN 2017. CCIS, vol. 720, pp. 94–105. Springer, Cham (2017). https://doi.org/10.1007/978-3-319-71011-2_8
19. Salcedo, V.S., Aguilar, W.G., Cobeña, B., Pardo, J.A., Proaño, Z.: On-board target virtualization using image features for UAV autonomous tracking. In: Boudriga, N., Alouini, M.-S., Rekhis, S., Sabir, E., Pollin, S. (eds.) UNet 2018. LNCS, vol. 11277, pp. 384–391. Springer, Cham (2018). https://doi.org/10.1007/978-3-030-02849-7_34
20. Fong, T., Thorpe, C.: Vehicle teleoperation interfaces. Auton. Robots **11**(1), 9–18 (2001)
21. Aguilar, W.G., Luna, M., Moya, J., Abad, V., Parra, H., Ruiz, H.: Pedestrian detection for UAVs using cascade classifiers with meanshift. In: IEEE 11th International Conference on Semantic Computing (ICSC), San Diego (2017)
22. Aguilar, W., Rodriguez, G., Álvarez, L.: On-board visual SLAM on a UGV using a RGB-D camera. Intell. Robot. Appl. **10464**, 298–308 (2017)
23. Amaguaña, F., Collaguazo, B., Tituaña, J.: Simulation system based on augmented reality for optimization of training tactics on military operations. Augment. Reality Virtual Reality Comput. Graph. **10850**, 298–308 (2017)
24. Aguilar, W.G., Manosalvas, J.F., Guillén, J.A., Collaguazo, B.: Robust motion estimation based on multiple monocular camera for indoor autonomous navigation of micro aerial vehicle. In: De Paolis, L.T., Bourdot, P. (eds.) AVR 2018. LNCS, vol. 10851, pp. 547–561. Springer, Cham (2018). https://doi.org/10.1007/978-3-319-95282-6_39
25. Aguilar, W.G., Abad, V., Ruiz, H., Aguilar, J., Aguilar-Castillo, F.: RRT-based path planning for virtual bronchoscopy simulator. In: De Paolis, L.T., Bourdot, P., Mongelli, A. (eds.) AVR 2017. LNCS, vol. 10325, pp. 155–165. Springer, Cham (2017). https://doi.org/10.1007/978-3-319-60928-7_13
26. Aguilar, W.G., Cobeña, B., Rodriguez, G., Salcedo, V.S., Collaguazo, B.: SVM and RGB-D sensor based gesture recognition for UAV control. In: De Paolis, L.T., Bourdot, P. (eds.) AVR 2018. LNCS, vol. 10851, pp. 713–719. Springer, Cham (2018). https://doi.org/10.1007/978-3-319-95282-6_50
27. RifaïM, H., Hua, D., Hamel, T., Morin, P.: Haptic-based bilateral teleoperation of underactuated unmanned aerial vehicles. IFAC Proc. Volumes (IFAC-PapersOnline) **44**, 13782–13788 (2011)
28. Lee, D., Franchi, A., Son, H.I., Ha, C., Heinrich, H., Giordano, P.R.: Semi-autonomous haptic teleoperation control architecture of multiple unmanned aerial vehicles. IEEE/ASME Trans. Mechatron. **18**, 1334–1345 (2013)
29. Lam, T., D'Amelio, V., Mulder, M., Van Paassen, M.M: UAV tele-operation using haptics with a degraded visual interface. In: Conference Proceedings - IEEE International Conference on Systems, Man and Cybernetics, vol. 3, pp. 2440–2445 (2007)
30. Chen, J.: UAV-guided navigation for ground robot tele-operation in a military reconnaissance environment. Ergonomics **53**(8), 940–950 (2010)
31. Galarza, J., Pérez, E., Serrano, E., Tapia, A., Aguilar, Wilbert G.: Pose estimation based on monocular visual odometry and lane detection for intelligent vehicles. In: De Paolis, L.T., Bourdot, P. (eds.) AVR 2018. LNCS, vol. 10851, pp. 562–566. Springer, Cham (2018). https://doi.org/10.1007/978-3-319-95282-6_40

32. Omari, S., Hua, M., Dueard, G., Hamel, T.: Bilateral haptic teleoperation of VTOL UAVs. In: IEEE International Conference on Robotics and Automation (ICRA), pp. 2393–2399 (2013)
33. Smisek, J., Sunil, E., Van Paassen, M.M., Abbink, D.A., Mulder, M.: Neuromuscular-system-based tuning of a haptic shared control interface for UAV teleoperation. IEEE Trans. Hum.-Mach. Syst. **47**(4), 449–461 (2017)
34. Kanso, A., Elhajj, I.H., Shammas, E., Asmar, D.: Enhanced teleoperation of UAVs with haptic feedback. In: IEEE/ASME International Conference on Advanced Intelligent Mechatronics, AIM, pp. 305–310 (2015)
35. Lee, D., Franchi, A., Giordano, P., Son, H., Bülthoff, H.H.: Haptic teleoperation of multiple unmanned aerial vehicles over the internet. In: Proceedings - IEEE International Conference on Robotics and Automation, pp. 1341–1347 (2011)
36. Guoqin, G.: Navigating path recognition for greenhouse mobile robot based on K-means algorithm. Trans. Chin. Soc. Agric. Eng. **30**, 25–33 (2014)
37. Al-kaff, A., Meng, Q., Mart, D.: Monocular vision-based obstacle detection/avoidance for unamnned aerial vehicles. In: IEEE Intelligent Vehicles Symposium (2016)
38. De Cristóforis, P., Nitsche, M.A., Krajník, T., Mejail, M.: Real-time monocular image-based path detection: a GPU-based embedded solution for on-board execution on mobile robots. J. Real-Time Image Process. **11**(2), 335–348 (2016)
39. Aguilar, W., Casaliglla, V., Pólit, J.: Obstacle avoidance based-visual navigation for micro aerial vehicles. Electronics **6**, 10 (2017)
40. Aguilar, W.G., et al.: Pedestrian detection for UAVs using cascade classifiers and saliency maps. In: Rojas, I., Joya, G., Catala, A. (eds.) IWANN 2017. LNCS, vol. 10306, pp. 563–574. Springer, Cham (2017). https://doi.org/10.1007/978-3-319-59147-6_48
41. Odelga, M., Stegagno, P., Bulthoff, H.H.: Obstacle detection, tracking and avoidance for a teleoperated UAV. In: Proceedings - IEEE International Conference on Robotics and Automation, pp. 2984–2990 (2016)
42. Aleotti, J., et al.: Detection of nuclear sources by UAV teleoperation using a visuo-haptic augmented reality interface. Sensors **17**(10), 1–22 (2017)